

*Supplementary material for*

**Phosphorescent iridium(III) complexes containing Ir-S-C-S structures for selective detection  
of Cu<sup>2+</sup> ions in solution and nanofibrous film**

Yi-Chuan Huang<sup>a</sup>, Xi Chu<sup>a</sup>, Shi-Sheng Zhao<sup>a</sup>, Wen-Hao Li<sup>a</sup>, Hong-Yan Li<sup>a\*</sup>, Wei Xue<sup>a, b\*</sup>

<sup>a</sup> *School of Chemical Engineering and Technology, Hebei University of Technology, Tianjin 300130, China*

<sup>b</sup> *Hebei Provincial Key Laboratory of Green Chemical Technology and High Efficient Energy Saving, Tianjin Key Laboratory of Chemical Process Safety*

---

\* Corresponding authors.

E-mail address: hyli@hebut.edu.cn (H.-Y. Li); weixue@hebut.edu.cn (W. Xue)

Contents

<i>Index</i>	<i>Page</i>
Experimental Section	S3
<b>Fig. S1-S9.</b> $^1\text{H}$ NMR and $^{13}\text{C}$ NMR spectra of $\text{L}_1$ - $\text{L}_3$ and <b>Ir1-Ir3</b> .	S8
<b>Fig. S10.</b> Cyclic voltammograms for complexes <b>Ir1-Ir3</b> in $\text{CH}_2\text{Cl}_2$ and MeCN solution at room temperature.	S12
<b>Fig. S11.</b> UV-vis spectra of <b>Ir1</b> (a) <b>Ir2</b> (b) and <b>Ir3</b> (c) ( $c = 2.0 \times 10^{-5} \text{ M}$ ) in the presence of various metal ions (2.0 equiv.) in MeCN. $\text{Ag}^+$ , $\text{Ca}^{2+}$ , $\text{Cd}^{2+}$ , $\text{Co}^{2+}$ , $\text{Cr}^{3+}$ , $\text{Fe}^{2+}$ , $\text{Fe}^{3+}$ , $\text{K}^+$ , $\text{Mg}^{2+}$ , $\text{Na}^+$ , $\text{Ni}^{2+}$ , $\text{Pb}^{2+}$ , $\text{Zn}^{2+}$ and $\text{Cu}^{2+}$ are added, respectively. Inset: the photos of before and after the $\text{Cu}^{2+}$ added in acetonitrile solution under chamber light.	S13
<b>Fig. S12.</b> Emission spectra of <b>Ir1</b> (a), <b>Ir2</b> (b) and <b>Ir3</b> (c) ( $5.0 \times 10^{-4} \text{ M}$ ) in the presence of 2.0 equiv. metal ions ( $\text{Ag}^+$ , $\text{Ca}^{2+}$ , $\text{Cd}^{2+}$ , $\text{Co}^{2+}$ , $\text{Cr}^{3+}$ , $\text{Fe}^{2+}$ , $\text{Fe}^{3+}$ , $\text{K}^+$ , $\text{Mg}^{2+}$ , $\text{Na}^+$ , $\text{Ni}^{2+}$ , $\text{Pb}^{2+}$ , $\text{Zn}^{2+}$ and $\text{Cu}^{2+}$ ) in acetonitrile solution.	S14
<b>Fig. S13.</b> Photo of 2.0 equivalent metal ions ( $\text{Ag}^+$ , $\text{Ca}^{2+}$ , $\text{Cd}^{2+}$ , $\text{Co}^{2+}$ , $\text{Cr}^{3+}$ , $\text{Fe}^{2+}$ , $\text{Fe}^{3+}$ , $\text{K}^+$ , $\text{Mg}^{2+}$ , $\text{Na}^+$ , $\text{Ni}^{2+}$ , $\text{Pb}^{2+}$ , $\text{Zn}^{2+}$ and $\text{Cu}^{2+}$ ) added into the acetonitrile solution of <b>Ir2</b> (a) and <b>Ir3</b> (b) under the irradiation of 365nm ultraviolet lamp.	S15
<b>Fig. S14.</b> The emission spectra of <b>Ir2</b> , <b>Ir2</b> + $\text{Cu}^{2+}$ (2.0 equiv.) and <b>Ir2</b> + $\text{Cu}^{2+}$ (2.0 equiv.) + $\text{Na}_2\text{EDTA}$ (2.0 equiv.) in acetonitrile solution.	S15
<b>Fig. S15.</b> Comparison chart in $^1\text{H}$ NMR ( $\text{DMSO}-d_6$ ) spectra of <b>Ir1</b> upon addition of 0, 2.0 equiv. of $\text{Cu}^{2+}$ .	S16
<b>Fig. S16.</b> The molecular structure of the complex <b>Ir2</b> and changes in $^1\text{H}$ NMR ( $\text{CD}_3\text{CN}$ ) spectra of <b>Ir2</b> upon addition of 0, 0.5, 1.0 and 2.0 equiv. of $\text{Cu}^{2+}$ .	S16
<b>Fig. S17.</b> The singlet and triplet DFT calculation summary results of $[(\text{L}_2)_2\text{Ir}(\text{MeCN})_2]^+$ .	S17
<b>Fig. S18.</b> Linear correlation between the concentration of $\text{Cu}^{2+}$ ions (0–10.0 $\mu\text{M}$ ) and emission intensities of <b>Ir1(a)/Ir2(b)/Ir3(c)</b> at their emission peaks.	S17
<b>Table S1.</b> Crystallographic data for complexes <b>Ir1</b> and <b>Ir3</b> .	S18
<b>Table S2.</b> Selected bond distances ( $\text{\AA}$ ) and angles ( $^\circ$ ) for complexes <b>Ir1</b> and <b>Ir3</b> .	S19
<b>Table S3.</b> The frontier orbital energy and electron density distribution for <b>Ir1-Ir3</b> .	S19
<b>Table S4.</b> Selected transitions from TD-DFT calculations of <b>Ir1</b> in the S1 state.	S20
<b>Table S5.</b> Selected transitions from TD-DFT calculations of <b>Ir2</b> in the S1 state.	S20
<b>Table S6.</b> Selected transitions from TD-DFT calculations of <b>Ir3</b> in the S1 state.	S20
<b>Table S7.</b> Phosphorescent emissions for the experimental reported Ir(III) complexes in acetonitrile media determined at the TD-B3LYP/6-31G(d)-LANL2DZ level of theory on the basis of the lowest triplet state geometry together with the experimental values.	S20
<b>Table S8.</b> Phosphorescent emissions for $[(\text{L}_2)_2\text{Ir}(\text{MeCN})_2]^+$ determined at the TD-B3LYP/6-31G(d)-LANL2DZ level of theory on the basis of the lowest triplet state geometry.	S20
<b>Table S9.</b> The reported chemical sensors for detection of $\text{Cu}^{2+}$ ions based on iridium(III) complexes.	S21
References	S22

## 1. Experimental Section

### 1.1 Materials and Instruments

All commercial reagents were used without further purification unless otherwise indicated.  $\text{IrCl}_3 \cdot n\text{H}_2\text{O}$  was purchased from Kunming Borui Metal Materials Co. Ltd. Boric acid derivatives and 2-bromopyridine-5-carbaldehyde were purchased from Aladdin Reagents.  $\text{Cu}(\text{NO}_3)_2 \cdot 3\text{H}_2\text{O}$ ,  $\text{AgNO}_3$ ,  $\text{KNO}_3$ ,  $\text{NaNO}_3$ ,  $\text{Ca}(\text{NO}_3)_2 \cdot 4\text{H}_2\text{O}$ ,  $\text{Cd}(\text{NO}_3)_2 \cdot 4\text{H}_2\text{O}$ ,  $\text{Cr}(\text{NO}_3)_3 \cdot 9\text{H}_2\text{O}$ ,  $\text{Co}(\text{NO}_3)_2 \cdot 6\text{H}_2\text{O}$ ,  $\text{Mg}(\text{NO}_3)_2 \cdot 6\text{H}_2\text{O}$ ,  $\text{Pb}(\text{NO}_3)_2$ ,  $\text{Fe}(\text{NO}_3)_2$ ,  $\text{Fe}(\text{NO}_3)_3$ ,  $\text{Zn}(\text{NO}_3)_2 \cdot 6\text{H}_2\text{O}$  and  $\text{Ni}(\text{NO}_3)_2 \cdot 6\text{H}_2\text{O}$  were purchased from Tianjin Kermel Chemical Reagent Company.

$^1\text{H}$  and  $^{13}\text{C}$  NMR spectra were measured on a Bruker AM 400 spectrometer. Deuterated reagents are  $\text{CDCl}_3$  and  $\text{DMSO}-d_6$ , chemical shift unit is ppm, multiplicity is expressed in s (singlet), d (doublet), t (triplet), and m (multiplet). The mass spectra (MS) were obtained using ESI-MS (Agilent 6520 Q-TOF LC/MS). The absorption spectra and photoluminescence spectra were recorded on UV-2700 spectrophotometer and Hitachi F-2700 photoluminescence spectrophotometer, respectively. The phosphorescence lifetimes of the complexes were measured using Edinburgh Instruments FLS920P fluorescence spectrometer in oxygen-free dichloromethane/acetonitrile solution at room temperature, and the data was fitted with Origin software.

The luminescence quantum efficiencies were calculated by comparison of the emission intensities (integrated areas) of a standard sample ( $\text{Ir}(\text{ppy})_3$ ) and the unknown sample according to the equation<sup>1,2</sup>.

$$\Phi_{\text{unk}} = \Phi_{\text{std}} \left( \frac{I_{\text{unk}}}{I_{\text{std}}} \right) \left( \frac{A_{\text{std}}}{A_{\text{unk}}} \right) \left( \frac{\eta_{\text{unk}}}{\eta_{\text{std}}} \right)^2$$

Where  $\Phi_{\text{unk}}$  and  $\Phi_{\text{std}}$  are the luminescence quantum yield of the unknown sample and  $\text{Ir}(\text{ppy})_3$ , respectively. The  $I_{\text{unk}}$  and  $I_{\text{std}}$  are the integrated emission intensities of the unknown sample and  $\text{Ir}(\text{ppy})_3$  solution, respectively. The  $A_{\text{unk}}$  and  $A_{\text{std}}$  are the absorbance of the unknown sample and  $\text{Ir}(\text{ppy})_3$  solution at their excitation wavelengths, respectively. The  $\eta_{\text{unk}}$  and  $\eta_{\text{std}}$  terms represent the refractive indices of the corresponding solvents (pure solvents were assumed). The  $\Phi_{\text{std}}$  of  $\text{Ir}(\text{ppy})_3$  measured in oxygen-free dichloromethane solution at room temperature has been revalued to be 0.97 (error:  $\pm 10\%$ )<sup>3,4</sup>.

### 1.2 Synthesis of Ligands and Complexes

Synthesis of cyclometalated ligands L<sub>1</sub>–L<sub>3</sub>.

6-phenylnicotinaldehyde (L<sub>1</sub>): Under nitrogen atmosphere, a mixture of phenylboronic acid (1.83 g, 15 mmol), 2-bromopyridine-5-carbaldehyde (1.86 g, 10 mmol), tetrakis(triphenylphosphine)palladium (0.17 g, 0.15 mmol) and sodium carbonate (4.25 g, 40 mmol) in THF and water (80 mL, 1:1, V/V) were refluxed for 24 h. After cooling to room temperature, the solvent was removed, and the obtained residue was purified by silica gel column chromatography (CH<sub>2</sub>Cl<sub>2</sub>/petroleum ether 1:2 (v/v)) to obtain white power with 1.54g. Yield: 84.25%. <sup>1</sup>H NMR (400 MHz, CDCl<sub>3</sub>) δ 10.28 – 10.06 (m, 1H), 9.14 (s, 1H), 8.24 (d, *J* = 8.0 Hz, 1H), 8.09 (d, *J* = 7.2 Hz, 2H), 7.92 (d, *J* = 8.2 Hz, 1H), 7.52 (d, *J* = 5.8 Hz, 3H).

6-(4-(trifluoromethyl)phenyl)nicotinaldehyde (L<sub>2</sub>): The synthesis procedure of L<sub>2</sub> is similar to that of L<sub>1</sub>, except that phenylboronic acid is replaced with 4-trifluoromethylphenylboronic acid. White powder was obtained with 2.06 g. Yield: 82.17%. <sup>1</sup>H NMR (400 MHz, CDCl<sub>3</sub>) δ 10.17 (s, 1H), 9.17 (s, 1H), 8.28 (dd, *J* = 8.2, 1.9 Hz, 1H), 8.21 (d, *J* = 8.1 Hz, 2H), 7.95 (d, *J* = 8.2 Hz, 1H), 7.78 (d, *J* = 8.2 Hz, 2H).

6-(4-methoxyphenyl)nicotinaldehyde (L<sub>3</sub>): Except for phenylboronic acid with 4-methoxyphenylboronic acid, the synthesis of L<sub>3</sub> is similar to that of L<sub>1</sub>. White powder was obtained with 1.84 g. Yield: 86.21%. <sup>1</sup>H NMR (400 MHz, CDCl<sub>3</sub>) δ 10.10 (s, 1H), 9.08 (d, *J* = 2.2 Hz, 1H), 8.18 (dd, *J* = 8.3, 2.2 Hz, 1H), 8.07 (d, *J* = 8.9 Hz, 2H), 7.84 (d, *J* = 8.4 Hz, 1H), 7.03 (d, *J* = 8.8 Hz, 2H), 3.89 (s, 3H).

Synthesis of Ir(III) complexes. A mixture of IrCl<sub>3</sub>·nH<sub>2</sub>O (0.18 g, 0.50 mmol) and three cyclometalated ligands (L<sub>1</sub>: 0.20 g, 1.1 mmol; L<sub>2</sub>: 0.28 g, 1.1 mmol; L<sub>3</sub>: 0.23 g, 1.1 mmol) in 2-ethoxyethanol and water (16 mL, 3: 1, v/v) were heated to 140 °C and refluxed for 24 h under nitrogen atmosphere. After cooling to room temperature and adding water, the precipitated chloro-bridged dimer was filtered without further purification. Then, the concentrated water solution of ancillary ligand salt NaCzdtc (1.2 mmol) was stirred with chloro-bridged dimer (1.0 mmol) in dichloromethane/methanol (1:1, v/v) at room temperature for 10 minutes. Then, the solution was concentrated, and the resulting residue was purified by silica gel column chromatography (CH<sub>2</sub>Cl<sub>2</sub>/MeOH 1: 1, v/v).

(L<sub>1</sub>)<sub>2</sub>Ir(Czdtc) (**Ir1**): red powder, 0.19 g, yield: 47.2%. <sup>1</sup>H NMR (400 MHz, DMSO-*d*<sub>6</sub>) δ 10.08 (s, 2H), 9.94 (s, 2H), 9.21 (d, *J* = 7.6 Hz, 2H), 8.44 (dd, *J* = 27.1, 8.4 Hz, 4H), 8.21 (d, 2H), 7.97 (d,

*J* = 7.6 Hz, 2H), 7.53 – 7.42 (m, 4H), 6.93 (t, *J* = 7.4 Hz, 2H), 6.82 (t, *J* = 7.1 Hz, 2H), 6.33 (d, *J* = 7.5 Hz, 2H).  $^{13}\text{C}$  NMR (101 MHz,  $\text{CDCl}_3$ )  $\delta$  219.36, 188.42, 173.91, 158.11, 156.01, 142.35, 139.57, 135.55, 131.72, 131.08, 130.73, 127.26, 126.90, 126.39, 124.84, 122.11, 119.61, 118.92, 118.15. ESI-MS calcd for  $[\text{C}_{37}\text{H}_{24}\text{IrN}_3\text{NaO}_2\text{S}_2]^+$  (822.0837); found 822.0841 [M + Na]<sup>+</sup>.

( $\text{L}_2$ )<sub>2</sub>Ir(Czdtc) (**Ir2**): red powder, 0.21 g, yield: 45.4%.  $^1\text{H}$  NMR (400 MHz,  $\text{DMSO}-d_6$ )  $\delta$  10.14 (s, 2H), 10.05 (s, 2H), 9.25 (d, *J* = 9.2 Hz, 2H), 8.68 (d, *J* = 8.5 Hz, 2H), 8.55 (d, *J* = 8.1 Hz, 2H), 8.23 (d, *J* = 7.8 Hz, 4H), 7.56 – 7.43 (m, 4H), 7.29 (d, *J* = 8.3 Hz, 2H), 6.49 (s, 2H).  $^{13}\text{C}$  NMR (101 MHz,  $\text{CDCl}_3$ )  $\delta$  218.83, 188.12, 172.37, 157.25, 155.57, 145.85, 139.62, 136.60, 131.89, 131.68, 131.58, 127.74 (q, *J* = 3.9 Hz), 127.51, 127.20, 126.19, 125.33, 120.06, 119.83, 119.38 (q, *J* = 3.8 Hz), 118.30. ESI-MS calcd for  $[\text{C}_{39}\text{H}_{23}\text{F}_6\text{IrN}_3\text{O}_2\text{S}_2]^+$  (936.0765); found 936.0760 [M + H]<sup>+</sup>.

( $\text{L}_3$ )<sub>2</sub>Ir(Czdtc) (**Ir3**): red powder, 0.18 g, yield: 42.6%.  $^1\text{H}$  NMR (400 MHz,  $\text{CDCl}_3$ )  $\delta$  10.00 (s, 2H), 9.92 (d, *J* = 1.9 Hz, 2H), 9.41 – 9.31 (m, 2H), 8.18 (dd, *J* = 8.5, 2.0 Hz, 2H), 8.00 – 7.93 (m, 2H), 7.90 (d, *J* = 8.6 Hz, 2H), 7.71 (d, *J* = 8.7 Hz, 2H), 7.43 – 7.36 (m, 4H), 6.55 (dd, *J* = 8.7, 2.5 Hz, 2H), 5.94 (d, *J* = 2.5 Hz, 2H), 3.58 (s, 6H).  $^{13}\text{C}$  NMR (101 MHz,  $\text{CDCl}_3$ )  $\delta$  219.38, 188.34, 173.29, 161.60, 160.63, 156.17, 139.55, 135.43, 135.17, 129.61, 128.27, 127.25, 126.89, 124.83, 119.61, 118.11, 118.08, 116.37, 108.38, 54.83. ESI-MS calcd for  $[\text{C}_{39}\text{H}_{28}\text{IrN}_3\text{NaO}_4\text{S}_2]^+$  (882.1048); found 882.1060 [M + Na]<sup>+</sup>.

### 1.3 X-ray Crystallography

X-ray diffraction data were collected with Siemens (Bruker) Smart CCD diffractometer using monochromatic Mo K $\alpha$  radiation ( $\lambda=0.7103\text{\AA}$ ) at 113 K. Parameters data were collected with Smart software<sup>5</sup> and refined with SAINT. The structure was solved by direct methods using the program SHELXL-2018<sup>6</sup>. The positions of metal atoms and their first coordination spheres were located from direct-methods E-maps; other non-hydrogen atoms were found in alternating difference Fourier syntheses and least-squares refinement cycles and, during the final cycles, refined anisotropically. Hydrogen atoms were placed in calculated position and refined as riding atoms with a uniform value of Uiso.

### 1.4 Cyclic Voltammetry

Electrochemical measurements were performed with CHI 760E electrochemical workstation, with a polished Pt plate as the working electrode, platinum thread as the counter electrode and  $\text{AgNO}_3$  (0.010 M in  $\text{CH}_3\text{CN}$ )-Ag as the reference electrode, tetrabutylammonium

hexafluorophosphate (0.10 M) was used as the electrolyte, using ferrocene ( $\text{Fc}^+/\text{Fc}$ ) as the internal standard, and the scan rate is  $100 \text{ mV}\cdot\text{s}^{-1}$ .

### 1.5 Computational Details

Density functional theory (DFT) and time-dependent DFT (TD-DFT) calculations using B3LYP<sup>7-9</sup> functional were performed. The basis set used for C, H, N, O, S and F atoms was 6-31G (d, p) while the LanL2DZ basis set was employed for Ir atoms. Optimization and vibration data confirm that the structure is extremely small on the corresponding potential energy surface. The solvent effect of dichloromethane was taken into consideration using conductor like polarizable continuum model (C-PCM)<sup>10, 11</sup>. All these calculations were performed with Gaussian 09<sup>12</sup>.

### 1.6 Copper(II) Titration and Selective Experiments

The stock solutions (2.0 mM) of complexes **Ir1–Ir3** were prepared in acetonitrile and then diluted with acetonitrile to 0.5 mM and 20  $\mu\text{M}$  for titration and selective experiments. Stock solutions (0.05 M) of  $\text{Cu}^{2+}$  ion and other metal ions ( $\text{Ag}^+$ ,  $\text{Ca}^{2+}$ ,  $\text{Cd}^{2+}$ ,  $\text{Co}^{2+}$ ,  $\text{Cr}^{3+}$ ,  $\text{Fe}^{2+}$ ,  $\text{Fe}^{3+}$ ,  $\text{K}^+$ ,  $\text{Mg}^{2+}$ ,  $\text{Na}^+$ ,  $\text{Ni}^{2+}$ ,  $\text{Pb}^{2+}$  and  $\text{Zn}^{2+}$ ) were prepared in deionized water.  $\text{Cu}^{2+}$  ion (0–2.0 equiv.) was adding incrementally with a micropipet to the solution of **Ir1–Ir3** in quartz cuvette to perform the titration experiments. The cation-competition experiments were performed by adding 2.0 equiv.  $\text{Cu}^{2+}$  ion into the mixture solution of Ir(III) complexes and the other metal ions. All the experiments were measured after standing for 5 minutes.

### 1.7 Determination of detection limit

The detection limit is calculated based on phosphorescence titration. The phosphorescence emission spectra of the complexes **Ir1–Ir3** were measured 10 times, and the standard deviation of the blank measurement was obtained. Plot the ratio of emission intensity to different ion concentrations to obtain the slope. The detection limit is calculated by the following formula<sup>13, 14</sup>.

$$\text{Detection limit} = \frac{3\sigma}{k}$$

Where  $\sigma$  is the standard deviation of the blank measurement, and  $k$  is the slope of the ratio of emission intensity to ion concentration.

### 1.8 Preparation of iridium complexes-composite nanofibrous film by electrospinning

Polyurethane (5.0 g) is dissolved in a mixed solution of tetrahydrofuran (10.0 g) and  $N,N'$ -dimethylformamide (10 g), heated and stirred at 60 °C for 12 hours to obtain a mixed fluid stand for use. After iridium complexes (1.0 mg) were dissolved in acetonitrile solution (1.0 g), the above-

mentioned fluid solution (9.0 g) were added thereto, and then the mixture were stirred at room temperature for 3 h. The precursor solution was loaded into a 5-mL gauge syringe with a push rate of 5 mL/h by peristaltic pump (Lead Fluid) under a high voltage of 12 kV to prepare nanofibers.

### 1.9 Fluorescence imaging

Fluorescence imaging were performed on Olympus IX83 Inverted Fluorescence Microscope. The luminescent signals were detected by the system of the confocal microscope with green channel (510-550 nm),  $\lambda_{\text{ex}} = 460\text{-}495 \text{ nm}$ , red channel (575-625 nm),  $\lambda_{\text{ex}} = 530\text{-}550 \text{ nm}$ .

### 1.10 Real water samples

Reagent water samples including tap, drinking and lake water from Hebei University of Technology, were filtered with a 0.2 mm filter membrane to remove large particles before use. Stock solutions of complexes **Ir1–Ir3** were prepared as described in titration experiment. Stock solutions (5.0 mM) of Cu<sup>2+</sup> were prepared in various actual water samples and were diluted to different concentration using actual samples. 2.00  $\mu\text{M}$  and 6.00  $\mu\text{M}$  of Cu<sup>2+</sup> ions were added to acetonitrile solution of complexes **Ir1–Ir3**, respectively, phosphorescence emission intensities were measured after standing for 5 minutes.

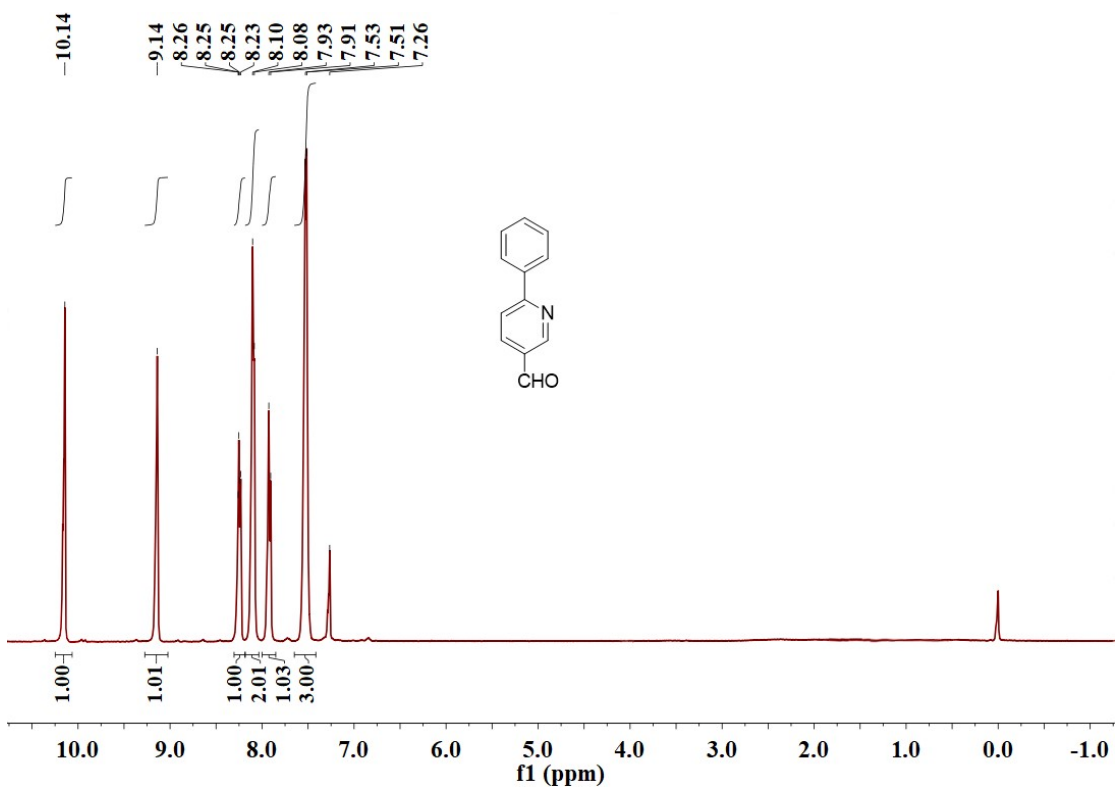


**Fig. S1.**  $^1\text{H}$  NMR spectrum of  $\text{L}_1$  in  $\text{CDCl}_3$  at 400 MHz at room temperature.

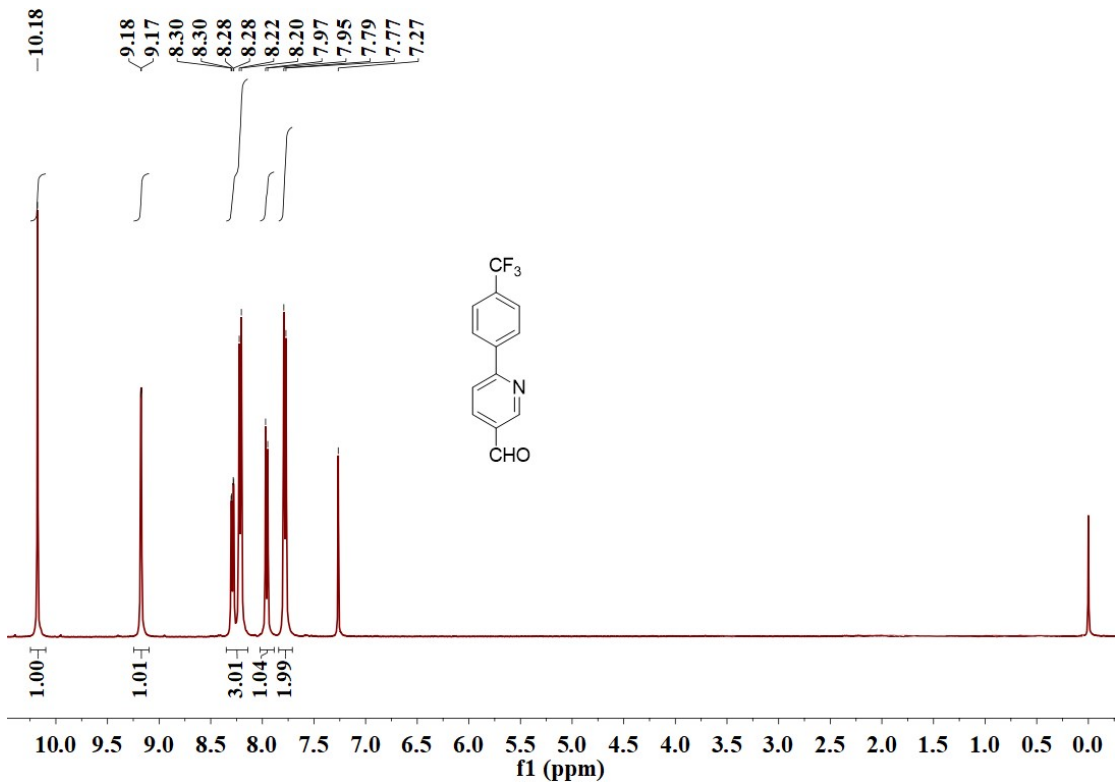


**Fig. S2.**  $^1\text{H}$  NMR spectrum of  $\text{L}_2$  in  $\text{CDCl}_3$  at 400 MHz at room temperature.

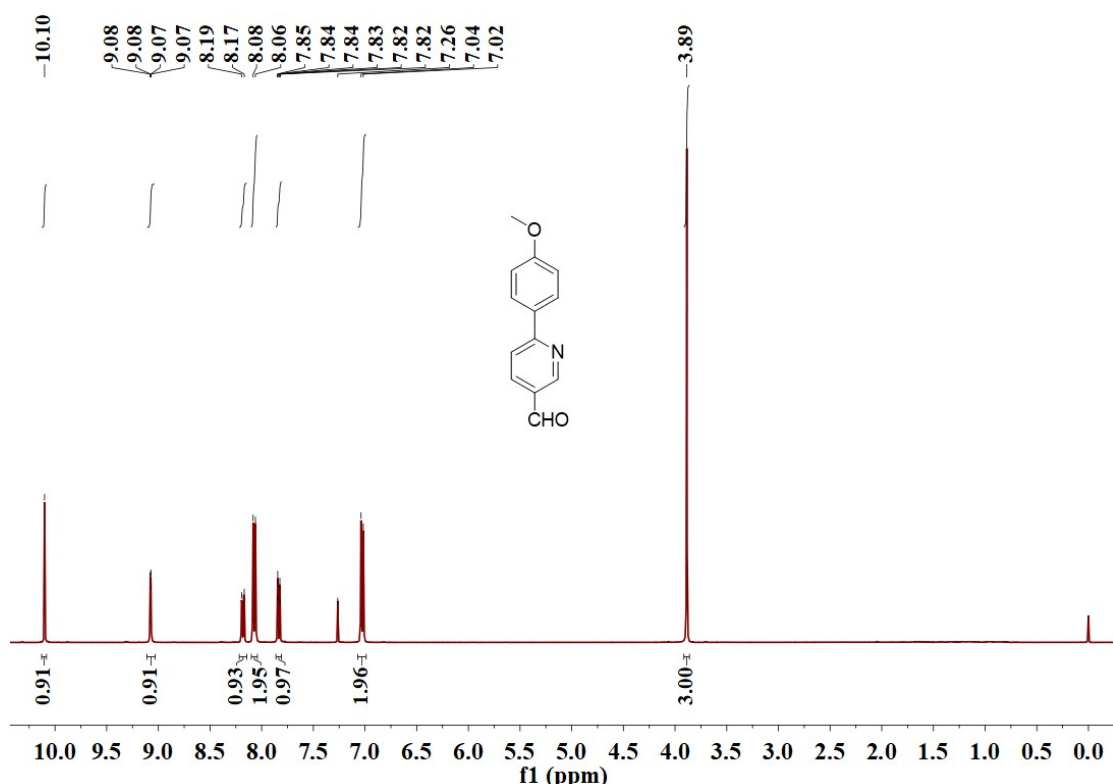


**Fig. S3.**  $^1\text{H}$  NMR spectrum of  $\mathbf{L}_3$  in  $\text{CDCl}_3$  at 400 MHz at room temperature.

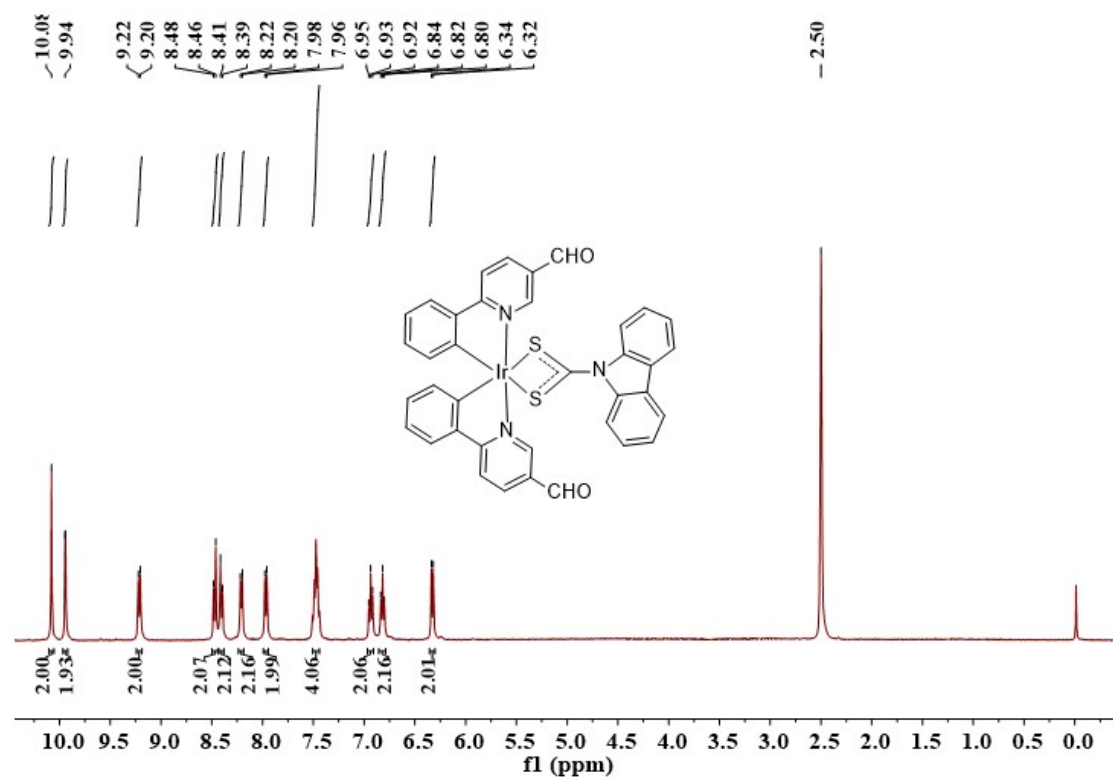


**Fig. S4.**  $^1\text{H}$  NMR spectrum of **Ir1** in  $\text{DMSO}-d_6$  at 400 MHz at room temperature.

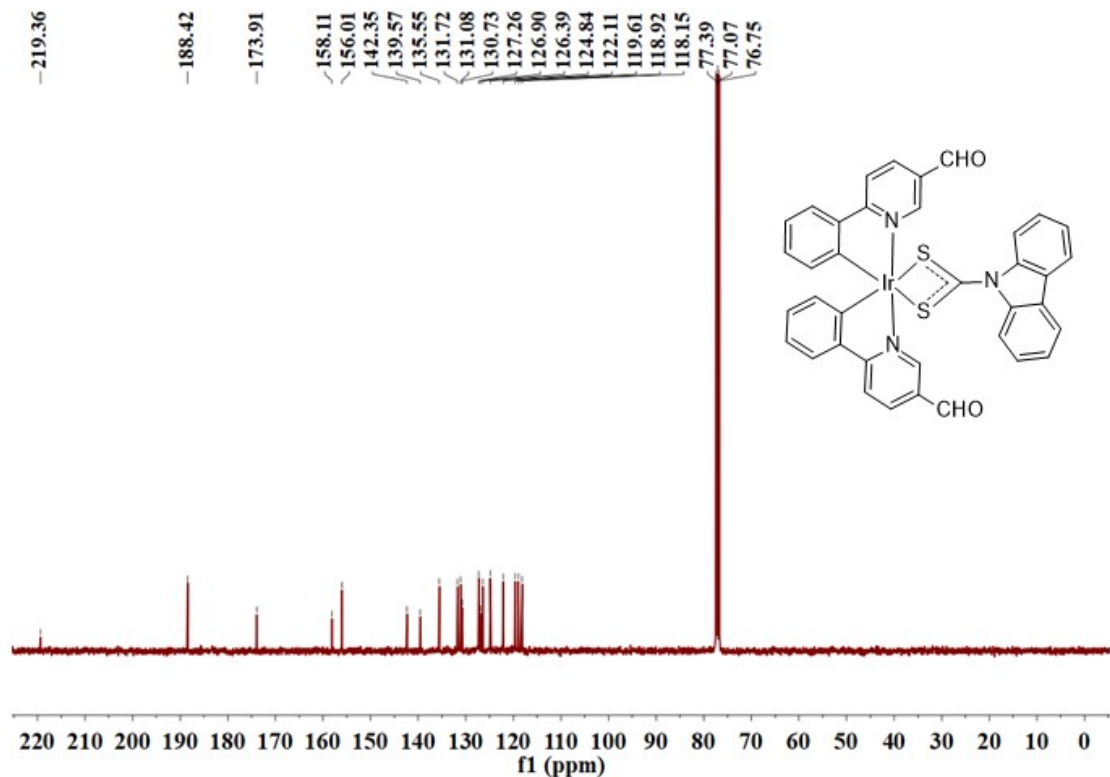


**Fig. S5.**  $^{13}\text{C}$  NMR spectrum of **Ir1** in  $\text{CDCl}_3$  at 101 MHz at room temperature.

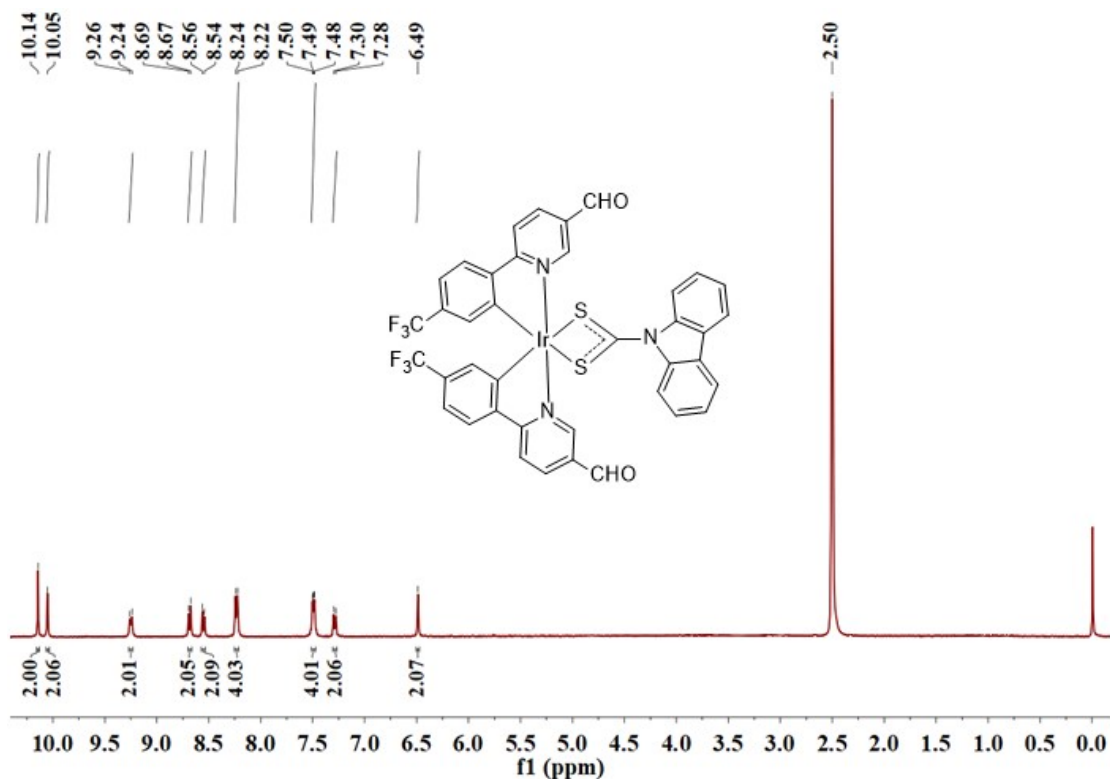


**Fig. S6.**  $^1\text{H}$  NMR spectrum of **Ir2** in  $\text{DMSO}-d_6$  at 400 MHz at room temperature.

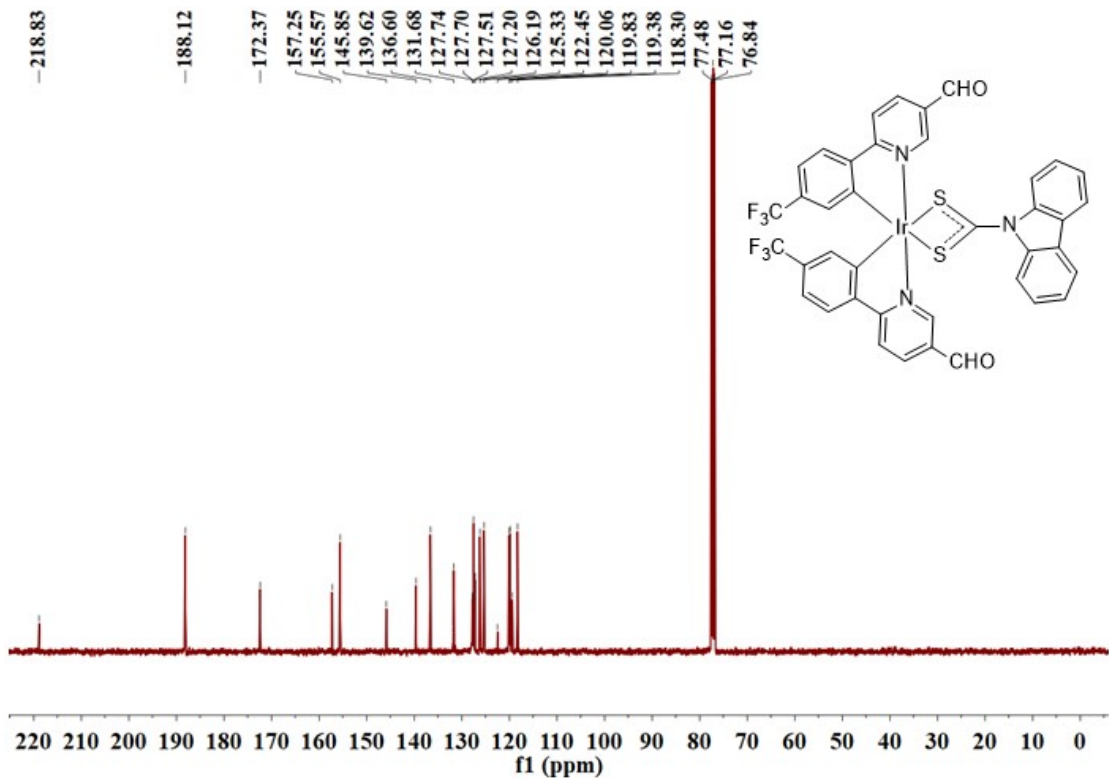


**Fig. S7.**  $^{13}\text{C}$  NMR spectrum of Ir2 in  $\text{CDCl}_3$  at 101 MHz at room temperature.

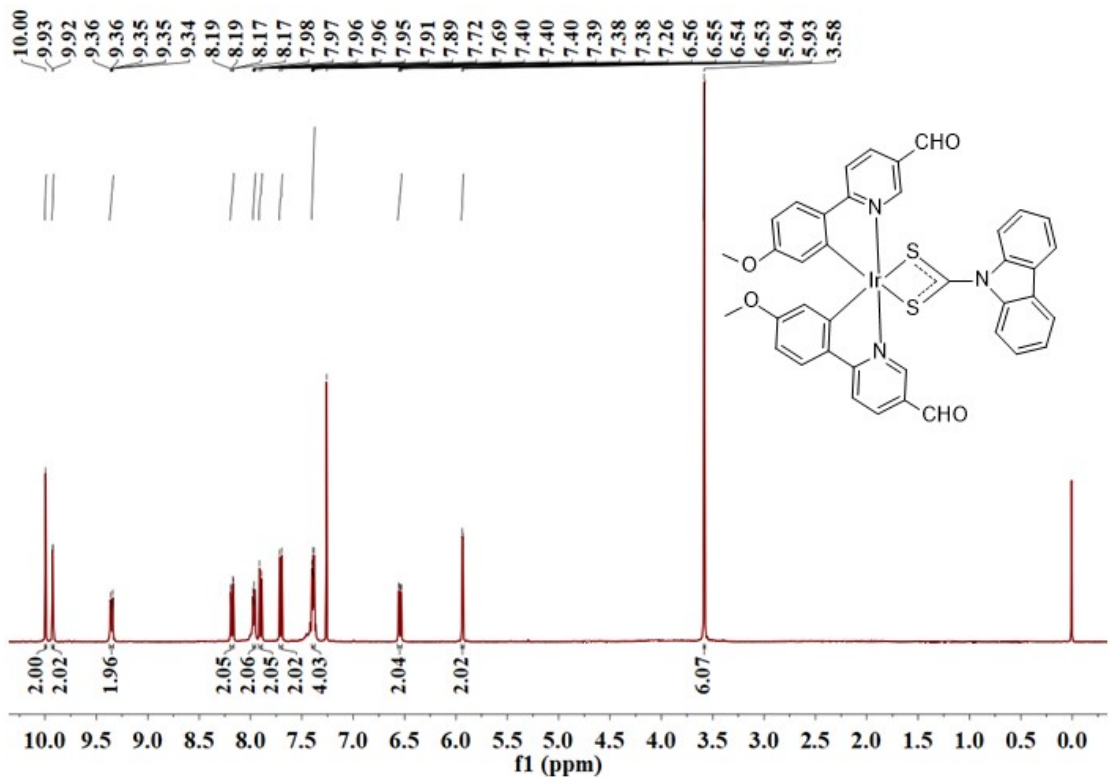


**Fig. S8.**  $^1\text{H}$  NMR spectrum of Ir3 in  $\text{CDCl}_3$  at 400 MHz at room temperature.

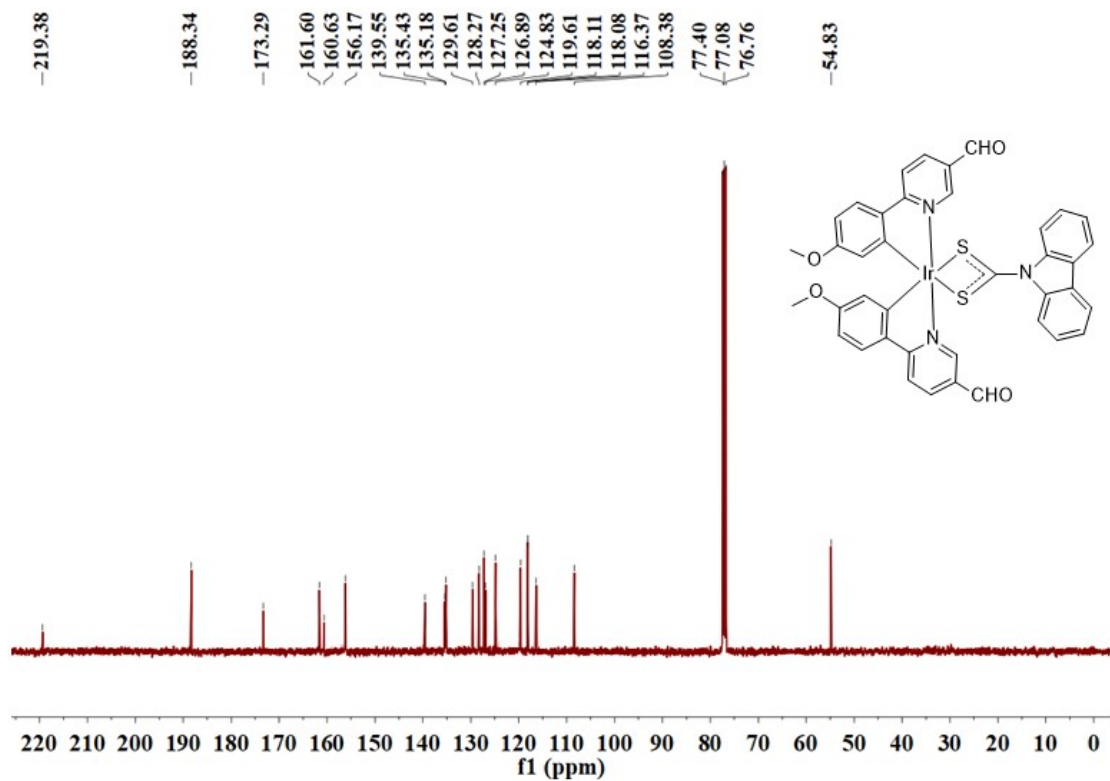


**Fig. S9.**  $^{13}\text{C}$  NMR spectrum of **Ir3** in  $\text{CDCl}_3$  at 101 MHz at room temperature.

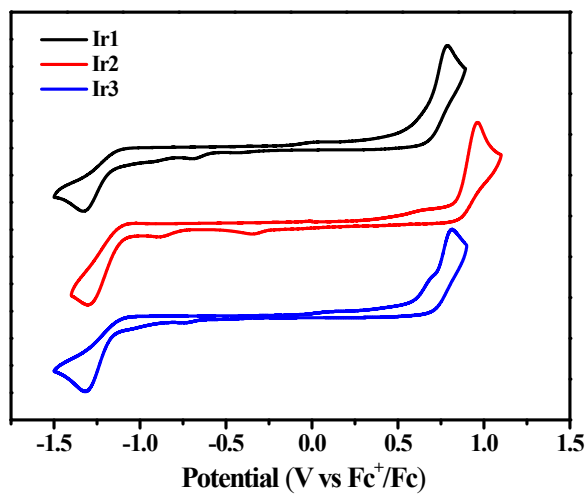


**Fig. S10.** Cyclic voltammograms for complexes **Ir1–Ir3** in  $\text{CH}_2\text{Cl}_2$  and MeCN solution at room temperature.

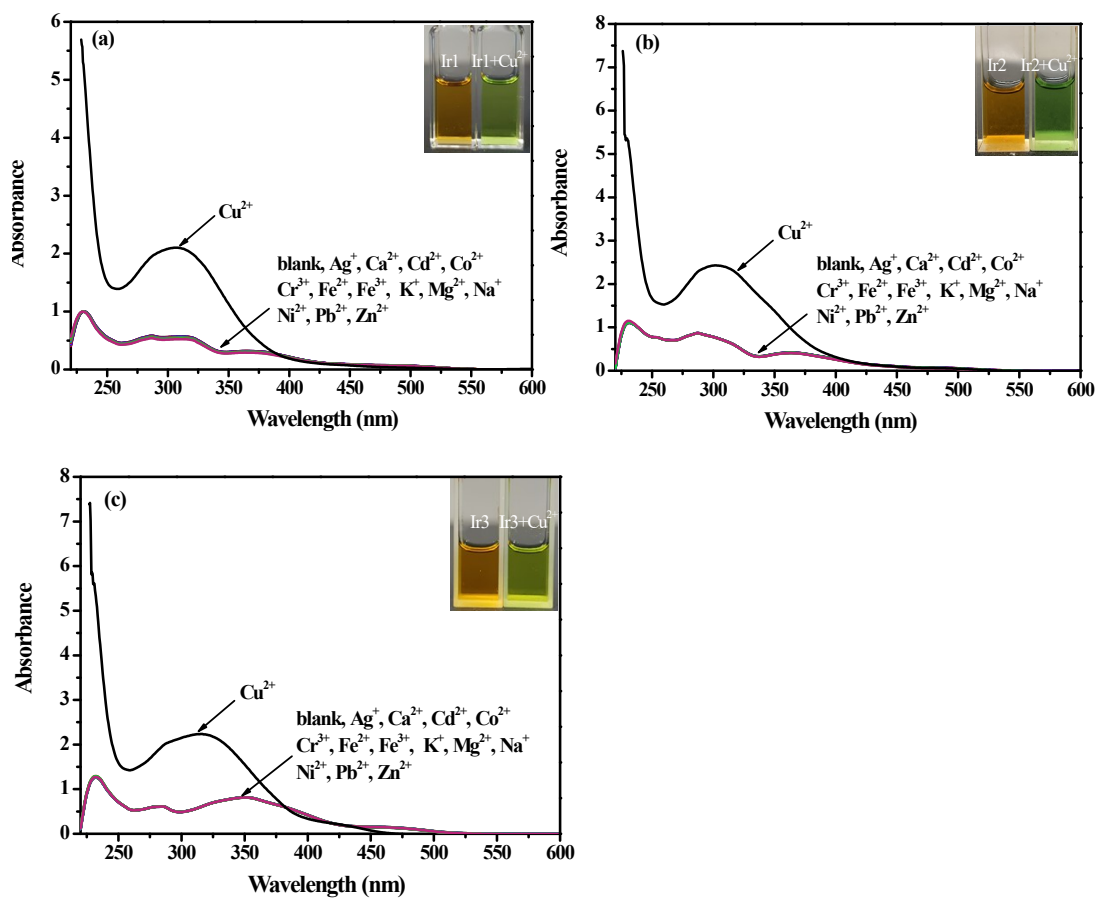


**Fig. S11.** UV-vis spectra of Ir1(a) Ir2(b) and Ir3(c) ( $c = 2.0 \times 10^{-5}$  M) in the presence of various metal ions (2.0 equiv.) in MeCN.  $\text{Ag}^+$ ,  $\text{Ca}^{2+}$ ,  $\text{Cd}^{2+}$ ,  $\text{Co}^{2+}$ ,  $\text{Cr}^{3+}$ ,  $\text{Fe}^{2+}$ ,  $\text{Fe}^{3+}$ ,  $\text{K}^+$ ,  $\text{Mg}^{2+}$ ,  $\text{Na}^+$ ,  $\text{Ni}^{2+}$ ,  $\text{Pb}^{2+}$ ,  $\text{Zn}^{2+}$  and  $\text{Cu}^{2+}$  are added, respectively. Inset: the photos of before and after the  $\text{Cu}^{2+}$  added in acetonitrile solution under chamber light.

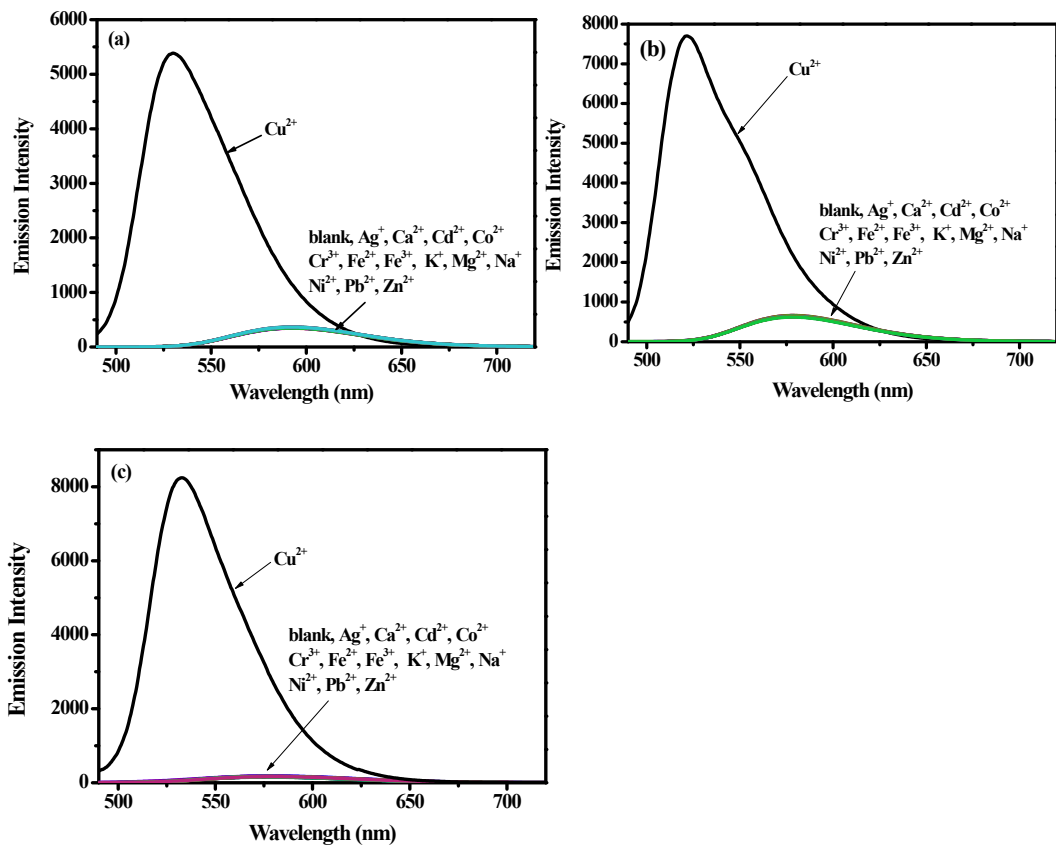


**Fig. S12.** Emission spectra of **Ir1**(a), **Ir2** (b) and **Ir3** (c) ( $5.0 \times 10^{-4}$  M) in the presence of 2.0 equiv. metal ions ( $\text{Ag}^+$ ,  $\text{Ca}^{2+}$ ,  $\text{Cd}^{2+}$ ,  $\text{Co}^{2+}$ ,  $\text{Cr}^{3+}$ ,  $\text{Fe}^{2+}$ ,  $\text{Fe}^{3+}$ ,  $\text{K}^+$ ,  $\text{Mg}^{2+}$ ,  $\text{Na}^+$ ,  $\text{Ni}^{2+}$ ,  $\text{Pb}^{2+}$ ,  $\text{Zn}^{2+}$  and  $\text{Cu}^{2+}$ ) in acetonitrile solution.

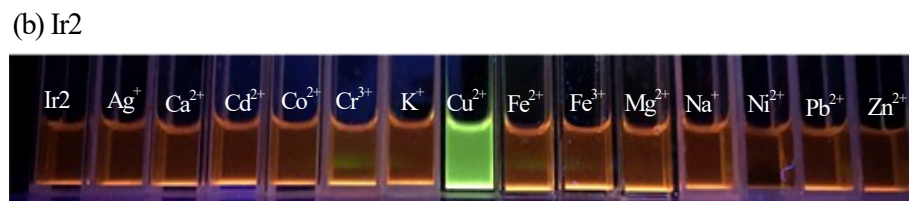
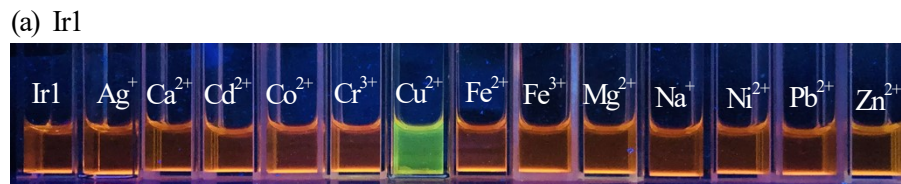


**Fig. S13.** Photos of 2.0 equivalent metal ions ( $\text{Ag}^+$ ,  $\text{Ca}^{2+}$ ,  $\text{Cd}^{2+}$ ,  $\text{Co}^{2+}$ ,  $\text{Cr}^{3+}$ ,  $\text{Fe}^{2+}$ ,  $\text{Fe}^{3+}$ ,  $\text{K}^+$ ,  $\text{Cu}^{2+}$ ,  $\text{Mg}^{2+}$ ,  $\text{Na}^+$ ,  $\text{Ni}^{2+}$ ,  $\text{Pb}^{2+}$  and  $\text{Zn}^{2+}$ ) added into the acetonitrile solution of **Ir1(a)**, **Ir2(b)** and **Ir3(c)** under the irradiation of 365 nm ultraviolet lamp.

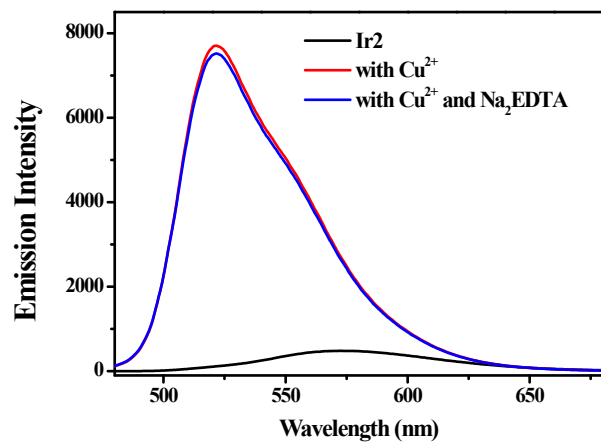


**Fig. S14.** The emission spectra of **Ir2**, **Ir2** +  $\text{Cu}^{2+}$  (2.0 equiv.) and **Ir2** +  $\text{Cu}^{2+}$  (2.0 equiv.) +  $\text{Na}_2\text{EDTA}$  (2.0 equiv.) in acetonitrile solution.

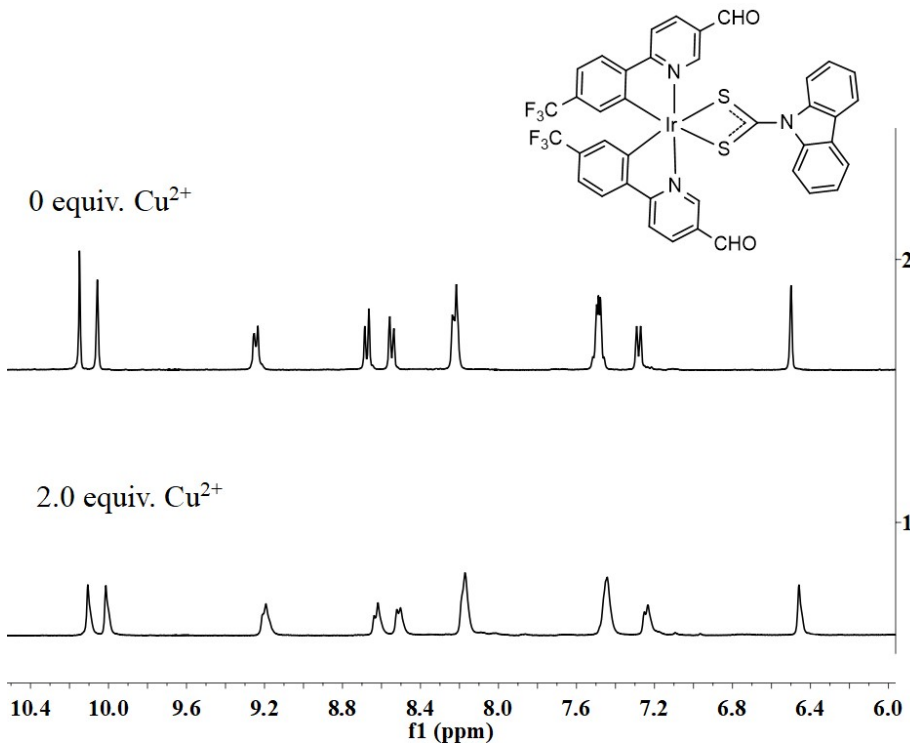


**Fig. S15.** Comparison chart in  $^1\text{H}$  NMR (DMSO- $d_6$ ) spectra of **Ir2** upon addition of 0, 2.0 equiv. of Cu $^{2+}$ .

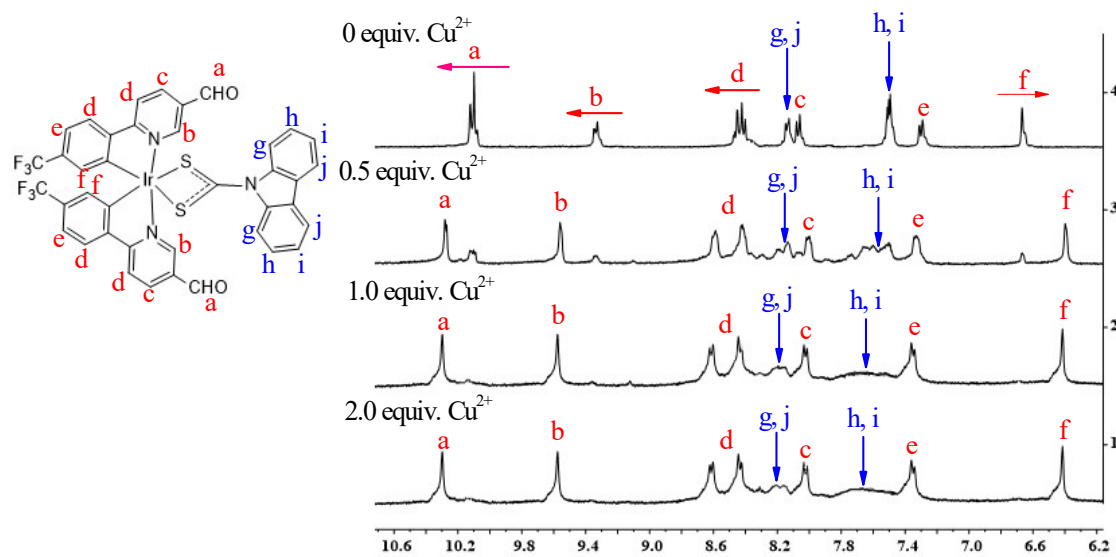


**Fig. S16.** The molecular structure of the complex **Ir2** and changes in  $^1\text{H}$  NMR ( $\text{CD}_3\text{CN}$ ) spectra of **Ir2** upon addition of 0, 0.5, 1.0 and 2.0 equiv. of Cu $^{2+}$ .

**G1:M2:V1 - Gaussian Calculation Summary**

File Name	pop-tfmppychomecn1-sol
File Type	.fch
Calculation Type	SP
Calculation Method	RB3LYP
Basis Set	GENECP
Charge	1
Spin	Singlet
Total Energy	-2228.41928162 a.u.
EBS Gradient Norm	0.00000000 a.u.
Imaginary Freq	
Dipole Moment	88.7918 Debyes
Point Group	

Ok View File Save Data .d1

**G2:M1:V1 - Gaussian Calculation Summary**

File Name	pop-tfmppychomecn3-sol
File Type	.fch
Calculation Type	SP
Calculation Method	UB3LYP
Basis Set	GENECP
Charge	1
Spin	Triplet
Total Energy	-2228.33214591 a.u.
EBS Gradient Norm	0.00000000 a.u.
Imaginary Freq	
Dipole Moment	87.6723 Debyes
Point Group	

Ok View File Save Data .d1

**Fig. S17.** The singlet and triplet DFT calculation summary results of  $[(L_2)_2\text{Ir}(\text{MeCN})_2]^+$ .

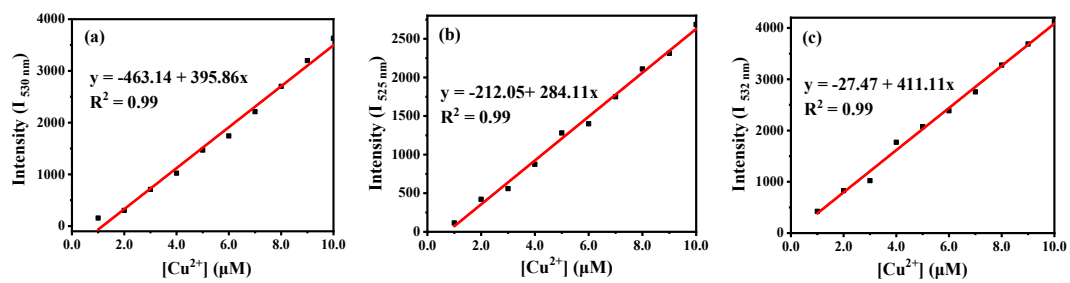


**Fig. S18.** Linear correlation between the concentration of  $\text{Cu}^{2+}$  ions (0–10.0  $\mu\text{M}$ ) and emission intensities of **Ir1(a)/Ir2(b)/Ir3(c)** at their emission peaks.

**Table S1** Crystallographic data for complexes **Ir1** and **Ir3**.

	<b>Ir1</b>	<b>Ir3</b>
Formula	C <sub>37</sub> H <sub>24</sub> IrN <sub>3</sub> O <sub>2</sub> S <sub>2</sub>	C <sub>39</sub> H <sub>28</sub> IrN <sub>3</sub> O <sub>4</sub> S <sub>2</sub>
W	798.91	858.960
T (K)	123.15	113.15
Wavelength (Å)	798.91	858.96
Cryst syst	monoclinic	monoclinic
Space group	P2(1)/c	Cc
<i>a</i> (Å)	14.3172(7)	16.0172(6)
<i>b</i> (Å)	18.2065(7)	25.5289(7)
<i>c</i> (Å)	12.7031(6)	9.3149(3)
$\alpha$ (deg)	90	90
$\beta$ (deg)	115.084(6)	103.618(4)
$\gamma$ (deg)	90	90
<i>V</i> (Å <sup>3</sup> )	2999.0(3)	3701.8(2)
<i>Z</i>	4	4
$\rho_{\text{calcd}}$ (g/cm <sup>3</sup> )	1.769	1.541
$\mu$ (Mo K $\alpha$ ) (mm <sup>-1</sup> )	4.632	3.762
<i>F</i> (000)	1568.0	1696.0
Range of transm factors (deg)	3.14-50.032	3.064 - 52.742
Reflns collected	28307	14826
Unique	5295	7012
GOF on <i>F</i> <sup>2</sup>	1.025	1.034
$R_I^{a,w}R_2^{b}$ ( $I > 2\sigma(I)$ )	0.0343, 0.0748	0.0381, 0.0755
$R_I^{a,w}R_2^{b}$ (all data)	0.0461, 0.0805	0.0421, 0.0788

**Table S2** Selected bond distances (Å) and angles (°) for complexes **Ir1** and **Ir3**.

<b>Ir1</b>					
Ir(1)-S(1)	2.45(13)	Ir(1)-S(2)	2.44(14)	Ir(1)-N(1)	2.04(4)
Ir(1)-N(2)	2.04(4)	Ir(1)-C(1)	2.02(5)	Ir(1)-C(2)	2.02(5)
S(1)-Ir(1)-S(2)	70.9(4)	N(1)-Ir(1)-S(1)	88.6(1)	N(1)-Ir(1)-S(2)	97.7(1)
N(1)-Ir(1)-N(2)	172.4(2)	N(2)-Ir(1)-S(1)	97.1(1)	N(2)-Ir(1)-S(3)	89.0(1)
C(1)-Ir(1)-S(1)	101.0(2)	C(1)-Ir(1)-S(2)	171.8(2)	C(1)-Ir(1)-N(1)	80.3(2)
C(1)-Ir(1)-N(2)	93.6(2)	C(2)-Ir(1)-S(1)	169.5(1)	C(2)-Ir(1)-S(2)	98.8(1)
C(2)-Ir(1)-N(1)	95.2(2)	C(2)-Ir(1)-N(2)	80.1(2)	C(1)-Ir(1)-C(2)	89.3(2)
<b>Ir3</b>					
Ir(1)-S(1)	2.47(4)	Ir(1)-S(2)	2.43(4)	Ir(1)-N(1)	2.04(2)
Ir(1)-N(2)	2.06(2)	Ir(1)-C(1)	1.96(2)	Ir(1)-C(2)	2.07(1)
S(2)-Ir(1)-S(1)	70.8(10)	N(1)-Ir(1)-S(1)	89.5(4)	N(1)-Ir(1)-S(2)	97.1(5)
N(1)-Ir(1)-N(2)	170.4(4)	N(1)-Ir(1)-C(2)	93.6(6)	N(2)-Ir(1)-S(1)	98.0(4)
N(2)-Ir(1)-S(2)	91.2(4)	N(2)-Ir(1)-C(2)	80.1(6)	C(1)-Ir(1)-S(1)	99.9(4)
C(1)-Ir(1)-S(2)	170.4(4)	C(1)-Ir(1)-N(1)	80.0(7)	C(1)-Ir(1)-N(2)	92.7(6)
C(1)-Ir(1)-C(2)	90.6(4)	N(2)-Ir(1)-S(1)	169.4(4)	C(2)-Ir(1)-S(2)	98.7(4)

**Table S3.** The frontier orbital energy and electron density distribution for **Ir1–Ir3**.

Complex	Orbital	Energy (eV) (Calculated)	$E_g$ (eV) (Calculated)	Composition %				
				-CF <sub>3</sub> / -OMe	phenyl	pyridine ring	Ir	Neutral ligands
<b>Ir1</b>	HOMO-2	-6.05	3.10	-	5.27	4.72	42.44	47.57
	HOMO-1	-5.96		-	2.68	3.78	24.19	69.35
	HOMO	-5.54		-	39.21	7.40	45.95	7.26
	LUMO	-2.44		-	17.96	78.38	1.91	1.75
	LUMO+1	-2.37		-	15.62	79.75	2.64	2.00
	LUMO+2	-1.99		-	0.78	2.47	2.89	93.85
<b>Ir2</b>	HOMO-2	-6.15	3.16	0.13	4.04	3.55	31.81	60.47
	HOMO-1	-6.02		0.03	1.84	2.81	17.87	77.45
	HOMO	-5.77		0.33	37.65	6.81	46.93	8.29
	LUMO	-2.62		1.81	20.26	73.98	1.75	1.69
	LUMO+1	-2.53		1.74	17.66	76.33	2.46	1.80
	LUMO+2	-2.05		0.01	0.94	2.60	2.89	93.57
<b>Ir3</b>	HOMO-2	-5.95	3.18	5.43	13.91	7.63	12.70	60.33
	HOMO-1	-5.85		14.72	35.58	18.70	13.29	17.60
	HOMO	-5.49		3.75	40.17	12.53	37.93	5.62
	LUMO	-2.31		2.97	15.86	78.08	1.43	1.66
	LUMO+1	-2.24		2.44	14.49	78.81	2.30	1.95
	LUMO+2	-1.97		0.01	1.01	2.46	2.88	93.64

**Table S4.** Selected transitions from TD-DFT calculations of **Ir1** in the S1 state.

$\lambda_{\text{abs}}(\text{nm})$ (Calcd)	$\lambda_{\text{abs}}(\text{nm})$ (Exptl)	Oscillator Strength	Major transition (s)	Character
499	496	0.1161	HOMO→LUMO (96%)	MLCT/LLCT/LC
377	372	0.1959	H-1→L+2 (82%)	MLCT/ILCT
319	314	0.0789	H-4→LUMO (28%), H-3→LUMO (47%)	LLCT/LC
306	286 231	0.2209	H-9→LUMO (73%)	LLCT/LC

**Table S5.** Selected transitions from TD-DFT calculations of **Ir2** in the S1 state.

$\lambda_{\text{abs}}(\text{nm})$ (Calcd)	$\lambda_{\text{abs}}(\text{nm})$ (Exptl)	Oscillator Strength	Major transition (s)	Character
490	490	0.1052	HOMO→LUMO (98%)	MLCT/LLCT
375	363	0.3173	H-1→L+2 (73%)	MLCT/ILCT
306	—	0.1049	H-9→L+1 (68%)	LLCT/LC
297	287	0.024	H-4→L+3 (80%)	LLCT
242	231	0.054	H-5→L+5 (71%)	MLCT/LLCT

**Table S6.** Selected transitions from TD-DFT calculations of **Ir3** in the S1 state.

$\lambda_{\text{abs}}(\text{nm})$ (Calcd)	$\lambda_{\text{abs}}(\text{nm})$ (Exptl)	Oscillator Strength	Major transition (s)	Character
477	475	0.1231	HOMO→LUMO (96%)	MLCT/LLCT
380	—	0.3172	H-2→L+2 (25%), H-1→L+2 (51%)	LLCT/LC
365	352	0.0991	HOMO→L+3(73%)	MLCT/LLCT
305	285	0.0022	HOMO→L+5(91%)	MLCT/LLCT
237	231	0.0401	H-16→L+1(71%)	LC

**Table S7.** Phosphorescent emissions for the experimental presented Ir(III) complexes in MeCN media determined at the TD-B3LYP/6-31G(d)-LANL2DZ level of theory on the basis of the lowest triplet state geometry.

Complex	State	AE (eV)	E (eV)	$\lambda(\text{nm})$	Major transition (s)	Description
<b>Ir1</b>	T <sub>1</sub>	2.18	2.12	584	HOMO→L+1 (91%)	<sup>3</sup> MLCT/ <sup>3</sup> LLCT
<b>Ir2</b>	T <sub>1</sub>	2.20	2.17	571	HOMO→L+1 (90%)	<sup>3</sup> MLCT/ <sup>3</sup> LLCT
<b>Ir3</b>	T <sub>1</sub>	2.23	2.28	543	H-1→L+1(24%) HOMO→L+1 (51%)	<sup>3</sup> LLCT/ <sup>3</sup> MLCT

**Table S8.** Phosphorescent emissions for [(L<sub>2</sub>)<sub>2</sub>Ir(MeCN)<sub>2</sub>]<sup>+</sup> determined at the TD-B3LYP/6-31G(d)-LANL2DZ level of theory on the basis of the lowest triplet state geometry.

	E(S <sub>1</sub> )	E(T <sub>1</sub> )	$\Delta E$	AE (eV)	$\lambda(\text{nm})$
[(L <sub>2</sub> ) <sub>2</sub> Ir(MeCN) <sub>2</sub> ] <sup>+</sup>	-2228.4193	-2228.3321	0.0872	2.36	525

**Table S9.** The reported chemical sensors for detection of Cu<sup>2+</sup> ions based on iridium(III) complexes.

Sample	Type	Limit of detection (M)	Reference
1 <sup>15</sup>	turn-off	–	<i>Inorg. Chem. Commun.</i> , <b>2012</b> , <i>16</i> , 1–3.
2 <sup>16</sup>	turn-off	–	<i>Bull. Korean Chem. Soc.</i> , <b>2013</b> , <i>34</i> , 653–656.
3 <sup>17</sup>	turn-off	–	<i>Tetrahedron Lett.</i> , <b>2013</b> , <i>54</i> , 779–782.
4 <sup>18</sup>	turn-off	10 <sup>-8</sup>	<i>Plos one</i> , <b>2014</b> , <i>9</i> , e99930.
5 <sup>19</sup>	turn-off	6.5 × 10 <sup>-5</sup>	<i>J. Lumin.</i> , <b>2016</b> , <i>177</i> , 299-305.
6 <sup>20</sup>	turn-off	7.6 × 10 <sup>-8</sup>	<i>J. Organomet. Chem.</i> , <b>2017</b> , <i>853</i> , 42-48.
7 <sup>21</sup>	turn-off	2.2 × 10 <sup>-8</sup>	<i>Dyes Pigm.</i> , <b>2019</b> , <i>161</i> , 252-260.
8 <sup>22</sup>	turn-off	2.7 × 10 <sup>-7</sup>	<i>Dyes Pigm.</i> , <b>2021</b> , <i>186</i> , 109016.
9 <sup>23</sup>	turn-off	1.1 × 10 <sup>-7</sup>	<i>Organometallics</i> , <b>2022</b> , <i>41</i> , 706-715.
10 <sup>24</sup>	turn-on	–	<i>Analyst</i> <b>2013</b> , <i>138</i> , 894-900.
<b>Ir1</b>	turn-on	3.31×10 <sup>-7</sup>	This paper
<b>Ir2</b>	turn-on	2.13×10 <sup>-7</sup>	This paper
<b>Ir3</b>	turn-on	1.74×10 <sup>-7</sup>	This paper

## References

- Frank, M.; Nieger, M.; Vögtle, F.; Belser, P.; von Zelewsky, A.; De Cola, L.; Balzani, V.; Barigelletti, F.; Flamigni, L. Dinuclear Ru(II) and/or Os(II) complexes of bis-bipyridine bridging ligands containing adamantane spacers: synthesis, luminescence properties, intercomponent energy and electron transfer processes, *Inorg. Chim. Acta.* **1996**, *242*, 281-291. [https://doi.org/10.1016/0020-1693\(95\)04878-2](https://doi.org/10.1016/0020-1693(95)04878-2).
- Juris, A.; Balzani, V.; Barigelletti, F.; Campagna, S.; Belser, P.; von Zelewsky, A. Ru(II) polypyridine complexes: photophysics, photochemistry, electrochemistry, and chemiluminescence, *Coord. Chem. Rev.* **1988**, *84*, 85-277. [https://doi.org/10.1016/0010-8545\(88\)80032-8](https://doi.org/10.1016/0010-8545(88)80032-8).
- Seo, H. J.; Song, M.; Jin, S. H.; Choi, J. H.; Yun, S. J.; Kim, Y. I. Blue phosphorescent iridium(iii) complexes containing carbazole-functionalized phenylpyridine for organic light-emitting diodes: energy transfer from carbazolyl moieties to iridium(iii) cores, *RSC Adv.* **2011**, *1*, 755. <https://doi.org/10.1039/C1RA00140J>.
- King, K. A.; Spellane, P. J.; Watts, R. J. Excited-state properties of a triply ortho-metallated iridium(III) complex, *J. Am. Chem. Soc.* **1985**, *107*, 1431-1432. <https://doi.org/10.1021/ja00291a064>.
- Sheldrick G. M. A short history of SHELX, *Acta Crystallogr., sect. A* **2008**, *64*, 112-122. <https://doi.org/10.1107/S0108767307043930>.
- Sheldrick G. M. SHELXTL-97, Universität of Göttingen, Göttingen, Germany. **1997**.
- Miehlich B.; Savin A.; Stoll H.; Preuss H. Results obtained with the correlation energy density functionals of Becke and Lee, Yang and Parr, *Chem. Phys. Lett.* **1989**, *157*, 200-206. [https://doi.org/10.1016/0009-2614\(89\)87234-3](https://doi.org/10.1016/0009-2614(89)87234-3).
- Becke A. D. Density-functional thermochemistry. III. the role of exact exchange, *J. Chem. Phys.* **1993**, *98*, 5648-5652. <https://doi.org/10.1007/s002149900065>.
- Cossi M.; Rega N.; Scalmani G.; Barone V.; Energies, structures, and electronic properties of molecules in solution with the C-PCM solvation model, *J. Comput. Chem.* **2003**, *24*, 669-681. <https://doi.org/10.1002/jcc.10189>.
- Tomasi J.; Mennucci B.; Cammi R. Quantum mechanical continuum solvation models, *Chem. Rev.* **2005**, *105*, 2999-3094. <https://doi.org/10.1021/cr9904009>.
- Lee C. T.; Yang W. T.; Parr R. G. Development of the Colle-Salvetti correlation-energy formula into a functional of the electron density, *Phys. Rev. B* **1988**, *37*, 785-789. <https://doi.org/10.1103/physrevb.37.785>.
- Frisch, M. J.; Trucks, G. W.; Schlegel, H. B.; Scuseria, G. E.; Robb, M. A.; Cheeseman, J. R.; Montgomery, J. J. A.; Vreven, T.; Kudin, K. N.; Burant, J. C.; Millam, J. M.; Iyengar, S. S.; Tomasi, J.; Barone, V.; Mennucci, B.; Cossi, M.; Scalmani, G.; Rega, N.; Petersson, G. A.; Nakatsuji, H.; Hada, M.; Ehara, M.; Toyota, K.; Fukuda, R.; Hasegawa, J.; Ishida, M.; Nakajima, T.; Honda, Y.; Kitao, O.; Nakai, H.; Klene, M.; Li, X.; Knox, J. E.; Hratchian, H. P.; Cross, J. B.; Adamo, C.; Jaramillo, J.; Gomperts, R.; Stratmann, R. E.; Yazyev, O.; Austin, A. J.; Cammi, R.; Pomelli, C.; Ochterski, J. W.; Ayala, P. Y.; Morokuma, K.; Voth, G. A.; Salvador, P.; Dannenberg, J. J.; Zakrzewski, V. G.; Dapprich, S.; Daniels, A. D.; Strain, M. C.; Farkas, O.; Malick, D. K.; Rabuck, A. D.; Raghavachari, K.; Foresman, J. B.; Ortiz, J. V.; Cui, Q.; Baboul, A. G.; Clifford, S.; Cioslowski, J.; Stefanov, B. B.; Liu, G.; Liashenko, A.; Piskorz,

- P.; Komaromi, I.; Martin, R. L.; Fox, D. J.; Keith, T.; Al-Laham, M. A.; Peng, C. Y.; Nanayakkara, A.; Challacombe, M.; Gill, P. M. W.; Johnson, B.; Chen, W.; Wong, M. W.; Gonzalez, C.; Pople, J. A. *Gaussian* **09**, **2010**.
13. Datta, B. K.; Thiagarajan, D.; Ramesh, A. A sole multi-analyte receptor responds with three distinct fluorescence signals: traffic signal like sensing of  $\text{Al}^{3+}$ ,  $\text{Zn}^{2+}$  and  $\text{F}^-$ , *Dalton Trans.* **2015**, *44*, 13093-13099. <https://doi.org/10.1039/C5DT01468A>.
  14. Ponram, M.; Balijapalli, U.; Sambath, B.; Kulathu Iyer, S.; Kakaraparthi, K.; Thota, G.; Bakthavachalam, V.; Cingaram, R.; Sung-Ho, J.; Natesan Sundaramurthy, K. Inkjet-printed phosphorescent Iridium(III) complex based paper sensor for highly selective detection of  $\text{Hg}^{2+}$ , *Dyes Pigm.* **2019**, *163*, 176-182. <https://doi.org/10.1016/j.dyepig.2018.11.054>.
  15. Yang, H.; Zhu, Y.; Li, L.; Zhou, Z.; Yang, S., A phosphorescent chemosensor for  $\text{Cu}^{2+}$  based on cationic iridium(III) complexes. *Inorganic Chemistry Communications* **2012**, *16*, 1-3. <https://doi.org/10.1016/j.inoche.2011.11.006>.
  16. Kim, H. B.; Li, Y.; Hyun, M. H., Phosphorescent chemosensor based on iridium(III) complex for the selective detection of  $\text{Cu}(\text{II})$  ion in aqueous acetonitrile. *Bull. Korean Chem. Soc.*, **2013**, *34* (2), 653-656. <https://doi.org/10.5012/bkcs.2013.34.2.653>.
  17. Lu, F.; Yamamura, M.; Nabeshima, T., Luminescent biscyclometalated iridium(III) complex for selective and switchable  $\text{Cu}^{2+}$  ion binding in aqueous media. *Tetrahedron Lett.*, **2013**, *54* (8), 779-782. <https://doi.org/10.1016/j.tetlet.2012.11.116>.
  18. Ma, D. L.; He, H. Z.; Chan, D. S. H.; Wong, C. Y.; Leung, C. H., A colorimetric and luminescent dual-modal assay for  $\text{Cu}(\text{II})$  ion detection using an iridium(III) complex. *PLoS One*, **2014**, *9* (6). <https://doi.org/10.1371/journal.pone.0099930>
  19. Shen, W.; Yan, L.; Tian, W.; Cui, X.; Qi, Z.; Sun, Y., A novel aggregation induced emission active cyclometalated Ir(III) complex as a luminescent probe for detection of copper(II) ion in aqueous solution. *J. Lumin.*, **2016**, *177*, 299-305. <https://doi.org/10.1016/j.jlumin.2016.04.048>.
  20. Yu, T.; Yang, Q.; Zhu, Z.; Zhao, Y.; Liu, X.; Wei, C.; Zhang, H., Synthesis, characterization and photophysical properties of a new  $\text{Cu}^{2+}$  selective phosphorescent sensor. *J. Organomet. Chem.*, **2017**, *853*, 42-48. <https://doi.org/10.1016/j.jorgancchem.2017.10.032>.
  21. Yu, T.; Wang, Y.; Zhu, Z.; Li, Y.; Zhao, Y.; Liu, X.; Zhang, H., Two new phosphorescent Ir(III) complexes as efficient selective sensors for the  $\text{Cu}^{2+}$  ion. *Dyes Pigm.*, **2019**, *161*, 252-260. <https://doi.org/10.1016/j.dyepig.2018.09.075>.
  22. Li, Z.; Ge, Z.; Tong, X.; Guo, L.; Huo, J.; Li, D.; Li, H.; Lu, A.; Li, T., Phosphorescent iridium(III) complexes bearing l-alanine ligands: Synthesis, crystal structures, photophysical properties, DFT calculations, and use as chemosensors for  $\text{Cu}^{2+}$  ion. *Dyes Pigm.*, **2021**, *186*, 109016. <https://doi.org/10.1016/j.dyepig.2020.109016>.
  23. Ge, Z. R.; Tong, X.; Huang, Y. C.; Li, W. H.; Li, H. Y.; Lu, A. D.; Li, T. Y., Highly luminescent dinuclear iridium(III) complexes containing phenanthroline-based neutral ligands as chemosensors for  $\text{Cu}^{2+}$  ion. *Organometallics*, **2022**, *41* (6), 706-715. <https://doi.org/10.1021/acs.organomet.1c00617>.
  24. Zhao, N.; Wu, Y. H.; Luo, J.; Shi, L. X.; Chen, Z. N., Aggregation-induced phosphorescence of iridium(iii) complexes with 2,2'-bipyridine-acetylhydrazone and their highly selective recognition to  $\text{Cu}^{2+}$ . *Analyst*, **2013**, *138* (3), 894-900. <https://doi.org/10.1039/C2AN36501D>.